Effects of niobium and titanium addition and surface treatment on electrical conductivity of 316 stainless steel as bipolar plates for proton-exchange membrane fuel cells

Seok-Hyun Lee [a,*], Jeong-Heon Kim [b,1], Min-Chul Kim [c,2], Dang-Moon Wee [a,3]

[a] Department of Materials Science and Engineering, KAIST, 373-1 Guseong Dong, Yuseong Gu, Daejeon 305-701, Republic of Korea
[b] R&D Center, Hankook Tire Co., Ltd., 23-1 Jangdong, Yuseong-gu, Daejeon 305-725, Republic of Korea
[c] Nuclear Materials Research Center, KAERI, P.O. Box 105, Yuseong-gu, Daejeon 305-353, Republic of Korea

ARTICLE INFO

ABSTRACT

Niobium and titanium are added to 316 stainless steel, and then heat treatment and surface treatment are performed on the 316 stainless steel and the Nb- and Ti-added alloys. All samples exhibit enhanced electrical conductivity after surface treatment but have low electrical conductivity before surface treatment due to the existence of non-conductive passive films on the alloy surfaces. In particular, the Nb- and Ti-added alloys experience a remarkable enhancement of electrical conductivity and cell performance compared with the original 316 stainless steel. Surface characterization reveals the presence of small carbide particles on the alloy surface after treatment, whereas the untreated alloys have a flat surface structure. $Cr_{23}C_6$ forms on the 316 stainless steel, and NbC and TiC forms on the Nb- and Ti-added alloys, respectively. The enhanced electrical conductivity after surface treatment is attributed to the formation of these carbide particles, which possibly act as electro-conductive channels through the passive film. Furthermore, NbC and TiC are considered to be more effective carbides than $Cr_{23}C_6$ as electro-conductive channels for stainless steel.

© 2008 Elsevier B.V. All rights reserved.

1. Introduction

The proton-exchange membrane fuel cell (PEMFC) is attracting much interest as an energy conversion device because it offers a higher coefficient of energy conversion than that of a conventional internal combustion engine, as well as having environmental advantages [1,2]. The bipolar plate is a key component in a PEMFC [3]. Many companies and institutes are using graphite plates as bipolar plates in research on fuel cells. The high cost of machining these graphite plates, however, is a practical obstacle to their widespread application [4,5].

Alternatively, metals appear to be good candidates for bipolar plates. This is because they can be easily deformed and have a better electrical conductivity than that of graphite. Recently, much research has been directed towards the development of metal-bipolar plates using austenite stainless steels, which have good corrosion resistance. 316 stainless steels are excellent candidate materials for bipolar plates due to their good corrosion behaviour in PEMFC environments [6–8]. Passivation of these steels may increase the contact resistance and reduce fuel cell performance [6]. Tarutani [9] reported that stainless steel in which Cr-base carbides were precipitated continuously maintained low contact resistance [9]. On the other hand, the precipitation of Cr-carbides, such as $Cr_{23}C_6$, causes the formation of a Cr-depleted zone adjacent to the grain boundaries and accelerated the corrosion of the stainless steel [10]. Thus, the inclusion of $Cr_{23}C_6$ is considered undesirable [11].

This study attempts to improve the interfacial contact conductance of metal-bipolar plates using austenite stainless steels by employing electrically conductive precipitates in 316 stainless steels (SS). Niobium and titanium are added to produce conductive precipitates in the 316SS and the interfacial contact conductance and the corrosion resistance are estimated. It is thought that the precipitates may play the role of a channel over the passive films and thereby allow the passage of electrical carriers.

2. Experimental procedure

2.1. Process details

The alloys used in this study (alloy 2 and alloy 3) were prepared from 316SS, and 316SS itself (alloy 1) was used in its original form as

* Corresponding author. Tel.: +82 42 350 4255; fax: +82 42 350 4275.
E-mail addresses: goodshjjang@kaist.ac.kr (S.-H. Lee), kimjh@hankooktire.com
(J.-H. Kim), mckim@kaeri.re.kr (M.-C. Kim), wee@kaist.ac.kr (D.-M. Wee).
1 Tel.: +82 42 865 0490; fax: +82 42 930 1478.
2 Tel.: +82 42 868 2000; fax: +82 42 868 2702.
3 Tel.: +82 42 350 4215; fax: +82 42 350 4275.

Table 1
Chemical composition of samples (wt.%).

	Chemical composition (wt.%) (Fe: balance)				
	Cr	Ni	C	Ti	Nb
Alloy 1	17	12	0.08	0	0
Alloy 2	17	12	0.08	0	3.0
Alloy 3	17	12	0.08	0.6	0

one of the studied alloys. Button ingots of approximately 90 g, which contained 3.0 wt.% Nb and 0.6 wt.% Ti, respectively, were prepared by vacuum arc melting under an argon atmosphere using a non-consumable tungsten electrode, and then remelted more than five times to ensure homogeneity. The chemical compositions of the three alloys compared in this study are given in Table 1. Solution treatment was carried out at 1300 °C in an argon atmosphere for 2 h. In order to precipitate carbides in each alloy, 2-h ageing treatment was applied at 840 °C for 316SS, 1050 °C for Nb-added 316SS, and 980 °C for Ti-added 316SS. Surface treatment was conducted after the ageing treatment. Al_2O_3 powder (particle size about 46 μm) used for shot blasting, and samples were pickled at 60 °C in a mixed acid solution (water + HF + HNO_3).

2.2. Interfacial contact resistance

The interfacial contact resistance (ICR) between each sample and its gas-diffusion layer (GDL) was measured with an ohm meter under simulated PEMFC conditions, as shown in Fig. 1, and as a function of compaction force [12]. A fixed electrical current (1 A) was passed through the arrangement and the potential difference was monitored as the compaction on the assembly was periodically increased (10–200 N cm^{-2}). The interfacial contact resistance was calculated as follows [13]:

$$ICR = \frac{R - R_G}{2} \times A \tag{1}$$

where R is the total resistance, R_G is the resistance between a copper plate and the GDL, and A is the area (1 cm^2). The ICR value of the copper plate|GDL interface was corrected by calibration. Therefore, the ICR results reported in this paper are only the corrected ICR values for the sample|GDL interface.

2.3. Single-cell tests

Single cells were assembled with catalyst-coated membranes, wet-proofed carbon papers, gaskets, and the prepared bipolar plates. To operate the single cells, 92–95% humidified hydrogen and air gases were fed to the anode and cathode, respectively. The stoichiometry of the H_2 and air was 1.5 and 2.0, respectively. The
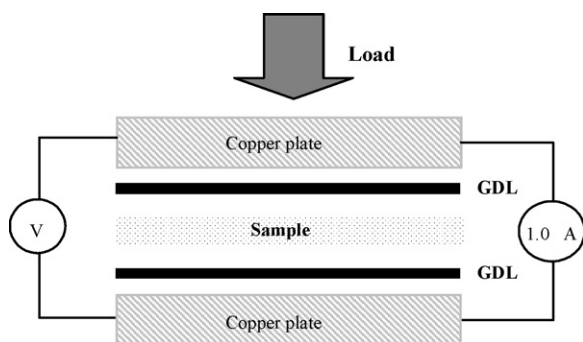

Fig. 1. Schematic illustration of test assembly for measuring interfacial contact resistance.

operating temperature and pressure were 66/65/62 (anode, cell, cathode) and 1 atm, respectively. The bipolar plates were of the 5-channel serpentine type.

3. Results and discussion

3.1. Microstructure characterization

Fig. 2(a), (b) and (c) shows the X-ray photoelectron spectroscopy (XPS) spectra of the surfaces of alloys 1, 2 and 3, respectively, before surface treatment. According to the narrow scanning spectra of alloy 1 shown in Fig. 2(a), the Cr 2p peak is present as an oxide, Cr_2O_3. No oxide peaks are apparent for Nb or Ti. According to the narrow scanning spectra of alloy 2 shown in Fig. 2(b), the Cr 2p peak is CrO_3. For Nb 3d and Ti 2p, Nb 3d represents Nb_2O_5 and Ti oxide peaks are not observed. Fig. 2(c) shows the narrow scanning spectra of alloy 3. For Cr 2p, the peaks are mainly of CrO_3, as in the case for alloy 2. For Nb 3d, no Nb oxide peaks are observed. For Ti 3d, the peaks are mainly those for TiO_2.

Fig. 3 shows scanning electron microscopy (SEM) images of the surfaces of alloy 1, alloy 2 and alloy 3 before and after surface treatments. The surface morphologies of the alloys are smooth and no precipitates are observed before surface treatment (Fig. 3(a)), but small precipitates (150–200 nm) are found after surface treatment (Fig. 3(b)–(d)). Energy dispersive spectrometer (EDS) analysis reveals that these precipitated particles are the Cr-rich phase (Fig. 4(a)), Nb-rich phase (Fig. 4(b)) and Ti-rich phase (Fig. 4(c)) for alloys 1, 2 and 3, respectively.

It is well known that chromium carbides (mainly $C_{23}C_6$) precipitate in grain boundaries when FeCrNi stainless steel is aged in the temperature range 400–850 °C. Thus, it can be seen that the Cr-rich precipitates (Fig. 4(a)) formed in alloy 1 (316SS) after ageing at 840 °C are Cr-carbides ($Cr_{23}C_6$). Both Nb and Ti, which strengthen carbides, are added to austenitic stainless steel in order to prevent the precipitation of Cr-carbides. As can be seen in Fig. 4(b), for the Nb-added alloy (alloy 2) aged at 1050 °C, only Nb-carbides (NbC) are formed in the matrix. As for Ti-added alloy (alloy 3) aged at 980 °C, only Ti-carbides (TiC) are formed (Fig. 4(c)). In the case of the Nb- and Ti-added alloys, the $Cr_{23}C_6$ carbides dissolve completely because the annealing time and temperature are sufficient [14–19]. These results indicate that, after ageing, $Cr_{23}C_6$, NbC and TiC are precipitated in alloy 1, alloy 2 and alloy 3, respectively. The carbides formed are projected into the surface after subsequent surface treatment.

3.2. Interfacial contact resistance

In our first experiments, we tested the interfacial contact resistance versus the compaction force of the three experimental alloys. Fig. 5 gives the interfacial contact resistance of each specimen before and after surface treatments. The ICR decreases with increasing compaction force for all samples. Further, the values for the specimens after surface treatment are lower throughout the range of compaction force (Fig. 5(a)). Before surface treatment, the contact resistance for alloys 1, 2 and 3 are approximately 25, 35 and 30 mΩ cm^2, respectively, at a compaction force of 140 N cm^{-2} (Fig. 5(b)). After surface treatment, the corresponding contact resistance is approximately 15, 10 and 10 mΩ cm^2 (Fig. 5(b)). This indicates that after surface treatment all samples showed a remarkable enhancement of electrical conductivity. Although before surface treatment the contact resistances of alloys 2 and 3 are higher than that of alloy 1, after surface treatment the contact resistances of alloys 2 and 3 are lower than that of alloy 1, as shown in Fig. 5(b). This indicates that surface treatment results in a greater improvement in electrical conductivity for alloys 2 and 3 than for alloy 1.

For stainless steel, the Cr-base protective oxide that forms on surface tends to yield a high value of the interfacial contact resistance, which can significantly degrade electrical performance [20]. Seo et al. [21] and Potgieter and Varga [22] reported that NbO_x and TiO_x are formed on Nb- and Ti-modified stainless steel, respectively, and Davies et al. [7] found a significant increase in ICR for 321SS (Ti added) and 347SS (Nb added). In our results, the con-

tact resistance for Nb- and Ti-added 316SS (alloy 2 and alloy 3) before surface treatment is higher than for the 316SS alone (alloy 1). This is attributed to the growth of an electrically insulating oxide film (Fig. 2). After surface treatment, however, the contact resistances for Nb- and Ti-added 316SS decrease significantly and are lower than that of the 316SS. This behaviour can be explained as follows. After surface treatment, the precipitates $Cr_{23}C_6$, NbC and
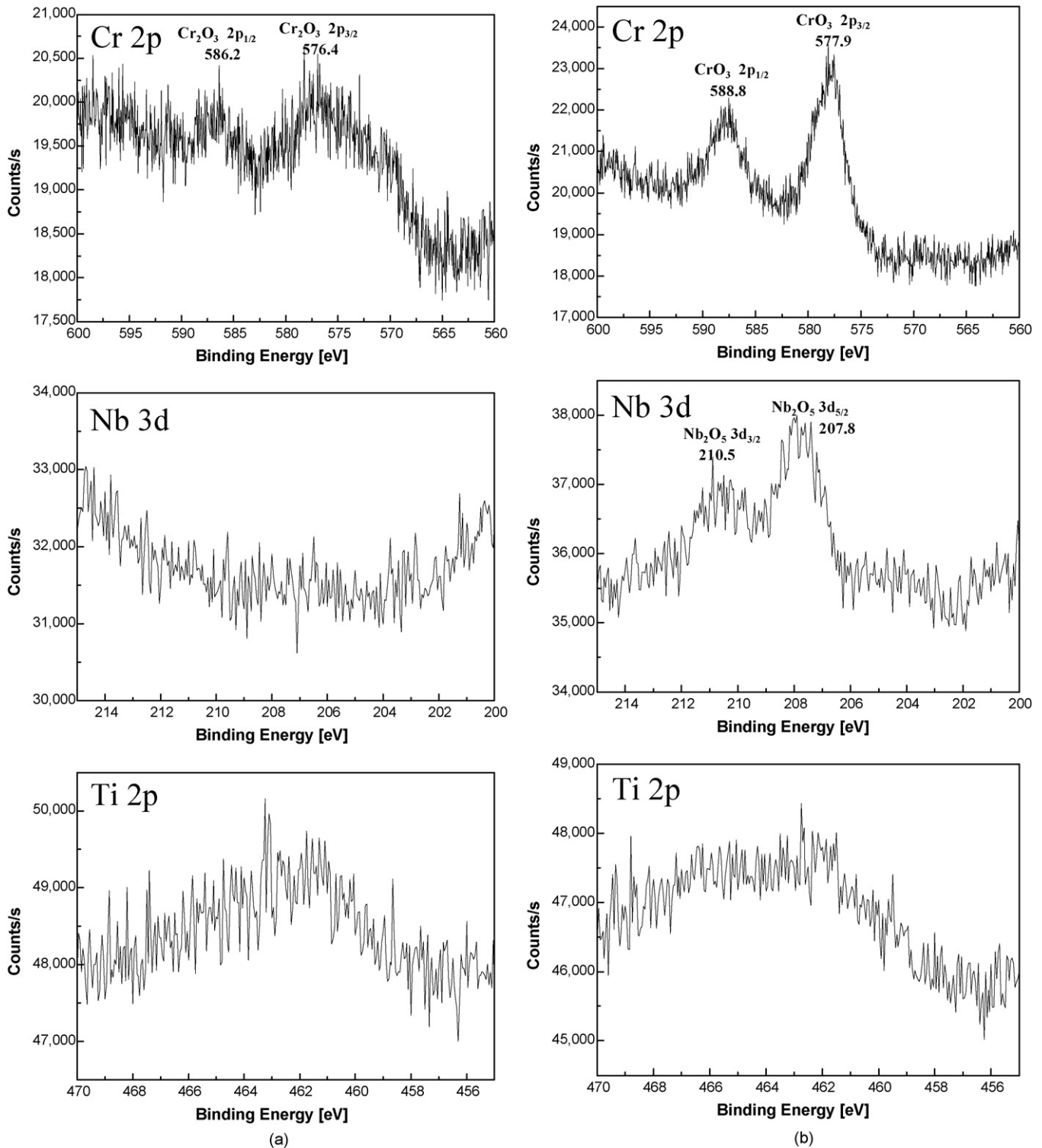

Fig. 2. XPS spectra for surfaces of (a) alloy 1, (b) alloy 2 and (c) alloy 3 before surface treatment.
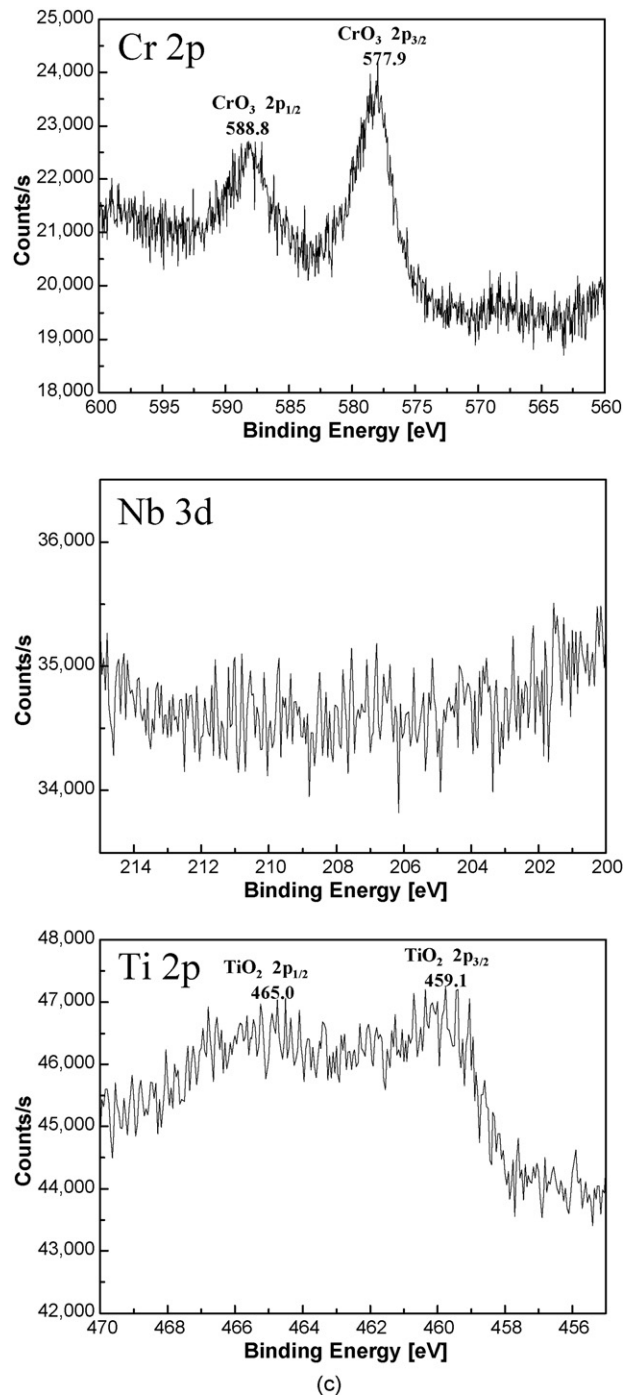
Fig. 2. (*Continued*).

TiC are dispersed and exposed on the surfaces of alloys 1, 2 and 3, respectively. These inclusions function as an electrical path and help to reduce the contact electrical resistance. Generally, carbides such as NbC, TiC and $Cr_{23}C_6$ have much better electrical conductivity than passive films [23]. Also, the electrical conductivities of MC-type carbides such as TiC and NbC are higher than those of $M_{23}C_6$-type carbides such as $Cr_{23}C_6$ [24,25]. In other words, TiC and NbC are more effective than $Cr_{23}C_6$ as electro-conducting channels on stainless steel; thus, alloy 2 with NbC and alloy 3 with TiC show lower contact resistance than alloy 1 with $Cr_{23}C_6$ after surface treatment.

3.3. Single-cell performance

Single cells of bare 316SS plates and the Nb- and Ti-added 316SS (alloy 2 and alloy 3) bipolar plates were assembled for tests of cell performance. The reaction area was 25 cm^2 and the fuels were pure hydrogen and air.

Fig. 6 presents the *I–V* and *I–P* curves of the single cells with graphite plates, 316SS plates and bipolar plates of alloys 2 and 3 (after ageing and surface treatment). At 0.6 V, the single cells employing alloy 2, alloy 3 and 316SS bipolar plates produce current densities of 672, 630 and 413 mA cm^{-2}, respectively. Alloy 2
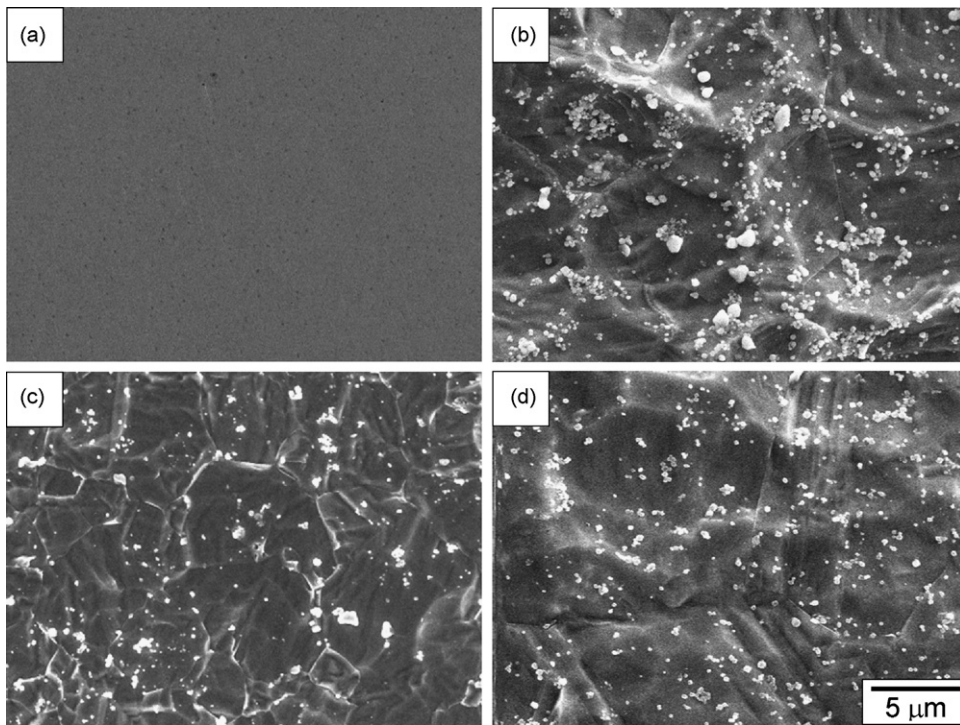
Fig. 3. Surface SEM images of alloy 1 (a) before and (b) after surface treatment and images of (c) alloy 2, and (d) alloy 3 after surface treatment.
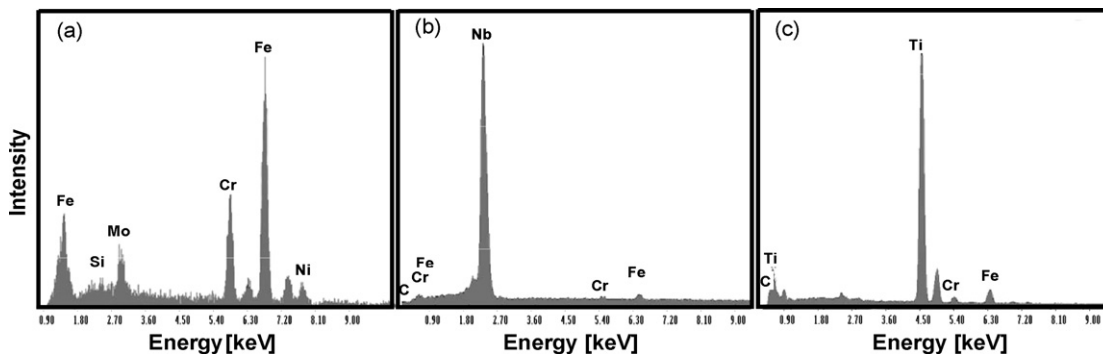

Fig. 4. EDS results obtained from small particles formed on (a) alloy 1, (b) alloy 2 and (c) alloy 3 after surface treatment.
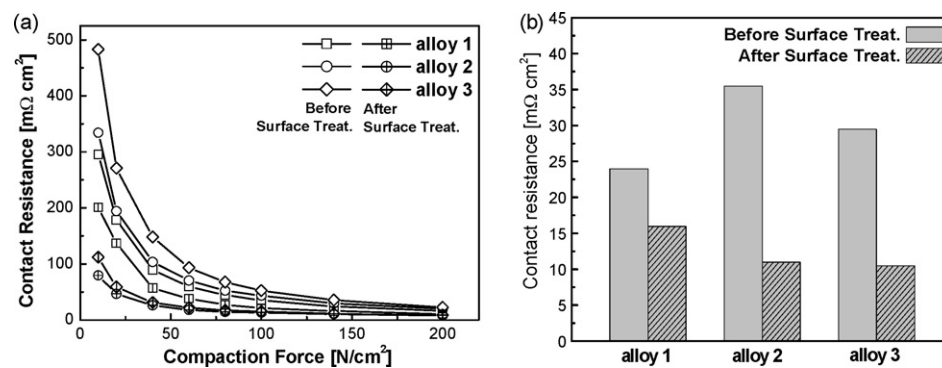

Fig. 5. Interfacial contact resistances of alloy 1, alloy 2 and alloy 3 (a) before and after surface treatment as a function of compaction force and (b) at compaction force 140 N cm^{-2}.
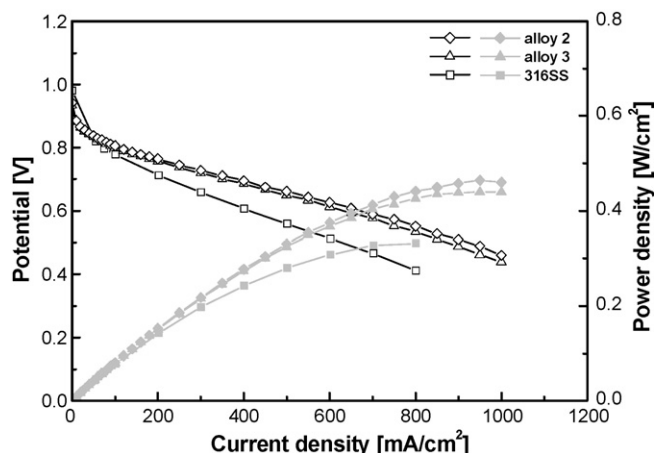
Fig. 6. Performance of unit cells of alloy 2, alloy 3 and 316SS.

and alloy 3 performed better than the 316SS. This is probably due to the lower contact resistance (Figs. 5 and 6).

4. Conclusions

In order to improve the electrical conductivity of 316SS, Nb and Ti are added and the resulting alloys are subjected to heat and surface treatment. The findings are listed below. These results suggest that Nb- and Ti-added 316SS are highly promising as bipolar plates for PEMFCs due to their enhanced electrical conductivity:

1. Cr oxide (Cr_2O_3) is mainly formed on the surface of 316SS before surface treatment. In the cases of Nb- and Ti-added 316SS, Cr oxide (CrO_3) is formed, and Nb oxide (Nb_2O_5) and Ti oxide (TiO_2), respectively, are also formed before surface treatment.
2. After surface treatment, all samples exhibit remarkable enhancement of electrical conductivity. The Nb- and Ti-added 316SS give greater enhancement of electrical conductivity than the original 316SS.
3. After ageing the samples, SEM observations reveal that NbC and TiC are precipitated in Nb- and Ti-added 316SS, respectively. The carbides are projected into the surface after subsequent surface

treatment. Also, Nb- and Ti-added 316SS have lower surface densities of carbide species than the original 316SS although they have a more enhanced electrical conductivity than the original alloys. These results suggest that NbC and TiC are more effective than $Cr_{23}C_6$ as electro-conducting channels on 316SS.

Acknowledgements

References

[1] S.J.C. Cleghorn, X. Ren, T. Espringer, M.S. Wilson, C. Zawodzinski, T.A. Azwodzinski, S. Gottesfeld, Int. J. Hydrogen Energy 22 (2002) 1137.
[2] J. Ihonen, F. Jaouen, G. Lindbergh, G. Sundholm, Electrochim. Acta 46 (2001) 2899.
[3] C.S. Kim, Polym. Sci. Tech 15 (2004) 550.
[4] E.A. Cho, I.H. Oh, Polym. Sci. Technol. 15 (2004) 612.
[5] I. Bar-On, R. Kirchain, R. Roth, J. Power Sources 102 (2002) 71.
[6] H. Wang, M. Sweikart, J.A. Turner, J. Power Sources 115 (2003) 243.
[7] D.P. Davies, P.L. Adcock, M. Turpin, S.J. Rowen, J. Appl. Electrochem. 30 (2000) 101.
[8] P.L. Hentall, J.B. Lakeman, Go. Mepsted, P.L. Adcock, J.M. Moore, J. Power Sources 80 (1999) 235.
[9] Y. Tarutani, Patent (USA) No. US6379476 B1, 2002.
[10] S.O. Cha, H.C. Choe, K.H. Kim, J. Kor. Inst. Met. Mater. 36 (1998) 138.
[11] J. Erneman, M. Schwind, P. Liu, J.O. Nilsson, H.O. Andren, J. Agren, Acta Mater. 52 (2004) 4337.
[12] D.P. Davies, P.L. Adcock, M. Turpin, S.J. Rowen, J. Power Sources 86 (2000) 237.
[13] R.F. Silva, D. Franchi, A. Leone, L. Pilloni, A. Masci, A. Pozio, Electrochim. Acta 51 (2006) 3592.
[14] H. Uno, A. Kimmura, T. Misawa, Corrosion 48 (1992) 467.
[15] J.H. Pater, R.W. Staehle, Corrosion 31 (1975) 30.
[16] C. Hoffmann, A.J. Mcevily, Metall. Trans. A 13A (1982) 923.
[17] M. Schwind, J. Kllqvist, J.O. Nilsson, J. Gren, H.O. Andrn, Acta Mater. 48 (2000) 2473.
[18] R.E. Hook, J.A. Elias, Metall. Trans. 3 (1972) 2171.
[19] M. Deighton, J. Iron Steel Inst. 11 (1970) 1012.
[20] J. Wind, R. Spah, W. Kaiser, G. Bohm, J. Power Sources 105 (2002) 256.
[21] M. Seo, G. Hultquist, C. Leygraf, N. Sato, Corros. Sci. 26 (1986) 949.
[22] J.H. Potgieter, K. Varga, Mater. Corros. 48 (1997) 221.
[23] Y.M. Chiang, D.P. Birnie, W.D. Kingery, Physical Ceramics: Principles for Ceramic Science and Engineering, John Wiley & Sons, Inc., Canada, 1997, pp. 185–262.
[24] V. Mazurovsky, M. Zinigrad, L. Leontiev, V. Lisin, Carbide formation during crystallization upon welding, http://www.yosh.ac.il/research/mmt/MMT-2004/papers/Section_3/3_126-133.doc, 2004.
[25] P.R. LeClair, Titanium nitride thin films by the electron shower process, http://bama.ua.edu/~pleclair/mit/thesis.pdf, 1998.